

# Macroscopic response in active nonlinear photonic crystals

Gandhi Alagappan,<sup>1,2,\*</sup> Sajeev John,<sup>1,3</sup> and Er Ping Li<sup>2</sup>

<sup>1</sup>Department of Physics, University of Toronto, 60 St. George Street, Toronto, Ontario M5S 1A7, Canada

<sup>2</sup>Institute of High Performance Computing, Fusionopolis, 1 Fusionopolis Way, No. 16-16 Connexis, Singapore 138632

<sup>3</sup>Department of Physics, King Abdulaziz University, Jeddah, Saudi Arabia

\*Corresponding author: alagapp@mailaps.org

Received May 21, 2013; revised July 6, 2013; accepted August 12, 2013;  
posted August 12, 2013 (Doc. ID 190806); published September 5, 2013

We derive macroscopic equations of motion for the slowly varying electric field amplitude in three-dimensional active nonlinear optical nanostructures. We show that the microscopic Maxwell equations and polarization dynamics can be simplified to a macroscopic one-dimensional problem in the direction of group velocity. For a three-level active material, we derive the steady-state equations for normal mode frequency, threshold pumping, nonlinear Bloch mode amplitude, and lasing in photonic crystals. Our analytical results accurately recapture the results of exact numerical methods. © 2013 Optical Society of America

OCIS codes: (050.5298) Photonic crystals; (190.0190) Nonlinear optics.

<http://dx.doi.org/10.1364/OL.38.003514>

Complex optical nanostructures such as photonic crystals (PCs) and PC-based devices can be doped with active constituents to produce nonlinear functionalities, such as lasing [1–4] or switching [5]. Active optical nanostructures can be modeled exactly using time-domain [3–5] or self-consistent frequency-domain methods [6,7]. The exact microscopic methods are time consuming (especially for a 3D structure) and do not provide a simple physical picture of the macroscopic nonlinear response. In this Letter, we provide a semi-analytical treatment of transient and steady-state response of 3D active optical nanostructures. Our semi-analytical treatment is not a perturbative approach [8] and is able to accurately recapture the results of more exact microscopic methods.

We assume the active optical nanostructure consists of a passive dielectric backbone structure and a region doped with active materials [6]. The dielectric function of the backbone structure is taken as  $\epsilon(\mathbf{r})$ , where  $\mathbf{r}$  is the position vector. The modes of the passive dielectric backbone structure satisfy the time-independent Maxwell equation,

$$\nabla \times \nabla \times \boldsymbol{\psi}_m(\mathbf{r}) - [\omega_m^2/c^2]\epsilon(\mathbf{r})\boldsymbol{\psi}_m(\mathbf{r}) = 0, \quad (1)$$

where  $\boldsymbol{\psi}_m(\mathbf{r})$  is the mode of the backbone with frequency  $\omega_m$ . In order to model the transient and steady-state behaviors of the active nanostructure, we model the active region with a complex nonlinear susceptibility  $\chi(\mathbf{r}, t)$  that varies slowly in time,  $t$  (compared with the optical period). Further, we assume the active material has only one resonance frequency for the radiative transitions. Assuming the resonance frequency of the active material is close to one of the backbone-mode frequencies (let say  $\omega_m$ ), we can write the electric field and polarization in the active optical nanostructure as

$$\mathbf{E}(\mathbf{r}, t) = A(\mathbf{r}, t)\boldsymbol{\psi}(\mathbf{r})e^{-i\omega t}, \quad (2)$$

$$\mathbf{P}(\mathbf{r}, t) = B(\mathbf{r}, t)\boldsymbol{\psi}(\mathbf{r})e^{-i\omega t}, \quad (3)$$

where  $\omega$  is the frequency of light, and  $A$  ( $B$ ) is a slowly varying electric field (polarization) amplitude. In writing Eqs. (2) and (3), we neglect the coupling between various backbone modes, and we suppress the subscript  $m$  in  $\boldsymbol{\psi}_m(\mathbf{r})$ . This assumption is justified below under suitable circumstances.

The electric field and polarization in Eqs. (2) and (3) obey the general time-dependent Maxwell equations,  $\nabla \times \mathbf{E} = \mu_0 \partial \mathbf{H} / \partial t$  and  $\nabla \times \mathbf{H} = \sigma(\mathbf{r})\mathbf{E} + \epsilon_0 \epsilon(\mathbf{r}) \partial \mathbf{E} / \partial t + \eta(\mathbf{r}) \partial \mathbf{P} / \partial t$ , where  $\mathbf{H}$  is the magnetic field,  $\sigma(\mathbf{r})$  is the conductivity that accounts for various losses (scattering, absorption, and finite sample size effects), and  $\eta(\mathbf{r})$  is the dimensionless function describing the location of the active material. The function  $\eta(\mathbf{r}) = 1$ , if active constituents are present at position  $\mathbf{r}$  and zero otherwise. To prevent the coupling between various modes of the backbone structure, the function  $\eta(\mathbf{r})$  is assumed to have the same symmetry as  $\epsilon(\mathbf{r})$ .  $\eta(\mathbf{r})$  can be nonzero both inside and outside the passive dielectric backbone.

Eliminating the magnetic field from the Maxwell equations, we have

$$\nabla \times \nabla \times \mathbf{E}(\mathbf{r}, t) + \frac{\epsilon(\mathbf{r})}{c^2} \frac{\partial^2 \mathbf{E}(\mathbf{r}, t)}{\partial t^2} + \mu_0 \sigma(\mathbf{r}) \frac{\partial \mathbf{E}(\mathbf{r}, t)}{\partial t} + \mu_0 \eta(\mathbf{r}) \frac{\partial^2 \mathbf{P}(\mathbf{r}, t)}{\partial t^2} = 0. \quad (4)$$

In order to obtain the equation of motion for  $A$ , we insert Eqs. (2) and (3) into Eq. (4) and impose an adiabatic limit. In the adiabatic limit,  $\partial B / \partial t \approx 0$  and  $B(\mathbf{r}, t) = \epsilon_0 \chi(\mathbf{r}, t) A(\mathbf{r}, t)$ . This approximation is valid when the polarization relaxation time is much shorter than the population decay time, as found in many physical systems [8–10]. For more details on adiabatic limits please see, for e.g., Refs. [9,10]. In the adiabatic limit,  $\partial B / \partial t \approx 0$  and  $B(\mathbf{r}, t) = \epsilon_0 \chi(\mathbf{r}, t) A(\mathbf{r}, t)$ . Assuming a small loss and neglecting the second-order terms (second-order derivatives of  $A$ , and term with  $\sigma \partial A / \partial t$  [10–12]), Eq. (4) becomes

$$\begin{aligned} & \nabla A \times \nabla \times \boldsymbol{\psi} + (\nabla A) \nabla \cdot \boldsymbol{\psi} - (\nabla A \cdot \nabla) \boldsymbol{\psi} \\ &= \frac{2i\omega}{c^2} \boldsymbol{\varepsilon} \boldsymbol{\psi} \frac{\partial A}{\partial t} + \frac{\omega^2}{c^2} \boldsymbol{\psi} A (i\gamma + \eta\chi + \delta\varepsilon). \end{aligned} \quad (5)$$

In Eq. (5), apart from  $\chi$ , we have dimensionless quantities  $\gamma = \sigma/(\varepsilon_0\omega)$  and  $\delta = 1 - \omega_m^2/\omega^2$ , quantifying the loss and the frequency detuning, respectively. In order to arrive at Eq. (5) from Eq. (4), we simplified the term  $\nabla \times \nabla \times \mathbf{E} = \nabla \times \nabla \times (\boldsymbol{\psi}A)$  in Eq. (4) using the vector identities:  $\nabla \times u\mathbf{V} \equiv \nabla u \times \mathbf{V} + u\nabla \times \mathbf{V}$  and  $\nabla \times (\mathbf{U} \times \mathbf{V}) \equiv \mathbf{U}(\nabla \cdot \mathbf{V}) - \mathbf{V}(\nabla \cdot \mathbf{U}) + (\mathbf{U} \cdot \nabla)\mathbf{V} - (\mathbf{V} \cdot \nabla)\mathbf{U}$  for a scalar function,  $u$  and vectors  $\mathbf{U}$  and  $\mathbf{V}$ . If we dot product the complex conjugate of  $\boldsymbol{\psi}$  on the left-hand side of Eq. (5), it follows that the dot product  $\boldsymbol{\psi}^* \cdot (\nabla A \times \nabla \times \boldsymbol{\psi} + (\nabla A) \nabla \cdot \boldsymbol{\psi} - (\nabla A \cdot \nabla) \boldsymbol{\psi})$  becomes  $\mathbf{q} \cdot \nabla A$ , where the Cartesian components of  $\mathbf{q} \equiv \mathbf{q}(\boldsymbol{\psi}, \boldsymbol{\psi}^*)$  in repeated index summation convention can be written as  $q_l = \psi_l^* \partial_j \psi_j - 2\psi_j^* \partial_l \psi_j + \psi_j^* \partial_j \psi_l$ , with  $\partial_i = \partial/\partial x_i$ . Here, the vector  $\mathbf{q}$  is physically significant. The direction of  $\mathbf{q}$  is the direction of group velocity, and the spatial average of  $\mathbf{q}$  is directly related to the group velocity  $\mathbf{v}_g = (ic^2/2\omega) \int_{-\infty}^{\infty} \mathbf{q} d^3\mathbf{r}$ . This expression for the group velocity is identical to the one obtained using a 3D  $\mathbf{k} \cdot \mathbf{p}$  perturbation theory [13]. Equation (5) now reduces to

$$i \frac{c^2}{2\omega} \mathbf{q} \cdot \nabla A + \boldsymbol{\varepsilon} \boldsymbol{\psi}^2 \frac{\partial A}{\partial t} = -\frac{\omega}{2} (i\gamma + \eta\chi + \delta\varepsilon) A \boldsymbol{\psi}^2. \quad (6)$$

Equation (6) describes the evolution of  $A$  both in time and space. If we choose our  $z$  axis parallel to the group velocity (i.e.,  $\mathbf{q}$ ), then the directional derivative  $\mathbf{q} \cdot \nabla A$  is proportional to  $\partial A/\partial z$ , reducing the original 3D problem [Eq. (4)] to a simpler 1D problem. Equation (6) can be discretized and solved using the first-order finite difference schemes, which is much easier than directly solving Eq. (4) [3,4]. It is likewise straightforward to generalize Eq. (6) to situations where Eqs. (2) and (3) involve an expansion over many coupled backbone modes.

If we further assume that the spatial variation of  $A$  is on much longer scales than the spatial variation of  $\boldsymbol{\psi}$ , then we can further simplify Eq. (6) by spatial averaging

$$v_g \cdot \nabla A + \frac{\partial A}{\partial t} = -\frac{\omega}{2} \{i\langle \gamma \boldsymbol{\psi}^2 \rangle + \langle \eta \chi \boldsymbol{\psi}^2 \rangle + \delta\} A. \quad (7)$$

In a PC,  $\langle \dots \rangle$  denotes  $(1/V_{\text{uc}}) \int_{\text{uc}} (\dots) d^3\mathbf{r}$ , where  $V_{\text{uc}}$  is the unit cell volume. In deriving Eq. (7), we use the normalization  $\langle \boldsymbol{\varepsilon} \boldsymbol{\psi}^2 \rangle = 1$ .

The dynamic Eqs. (6) and (7) are coupled to the equation of motion for  $\chi$ . In the case of active semiconductors,  $\chi$  is directly proportional to the number of free carriers and is governed by semiconductor Bloch equations or rate equations [14]. For active plasmonic materials, the dynamic equation for  $\chi$  can be obtained from particle-in-cell methods [15]. In the case of two-level atoms or quantum dots, the dynamic equation of  $\chi$  is described by the two-level optical Bloch equations [4,5,9,16], whereas for a general multilevel active dopant,  $\chi$  can be derived from the density matrix equations. Our simplified formalism, however, requires that there is only one radiative transition with strong coupling to our selected backbone

optical mode, whereas any other radiative transitions are weak [9].

We now consider the steady-state response of the macroscopic amplitude  $A$  under steady-state pumping conditions. In order to prevent the amplitude  $A$  from growing exponentially, the term on the right-hand side of Eq. (7) should be zero:  $i\langle \gamma \boldsymbol{\psi}^2 \rangle + \langle \eta \chi \boldsymbol{\psi}^2 \rangle + \delta = 0$ . By separating the imaginary (Im) and real (Re) parts of  $\chi$ , we find the steady-state conditions:

$$\langle \gamma \boldsymbol{\psi}^2 \rangle + \langle \eta \text{Im}(\chi) \boldsymbol{\psi}^2 \rangle = 0; \quad \langle \eta \text{Re}(\chi) \boldsymbol{\psi}^2 \rangle + \delta = 0. \quad (8)$$

For a specific illustration, consider a PC doped with active three-level atoms. Each active dopant is excited from level 1 to level 3 by means of an external pump [Fig. 1(a)]. Level 3 is assumed to nonradiatively decay rapidly to level 2. Radiation takes place between levels 2 and 1 with a frequency  $\omega_0$ . The complex susceptibility for such a three-level active medium is [6,7,16]:

$$\chi(\mathbf{r}) = g_0 \left( \frac{p-1}{p+1} \right) \frac{(\omega - \omega_0)T_2 - i}{1 + [(\omega - \omega_0)T_2]^2 + A^2 \boldsymbol{\psi}^2(\mathbf{r})/I_s(p+1)}, \quad (9)$$

where  $p$  is the pumping, defined as the ratio of pumping rate from level 1 to level 3 to the decay rate from level 2 to level 1,  $T_1$ . In Eq. (9),  $g_0$  is the maximum gain, and  $I_s$  is the saturation intensity. The expressions for  $g_0$  and  $I_s$  are  $d_0^2 T_2 N_T / (\varepsilon_0 \hbar)$  and  $\hbar^2 / (4d_0^2 T_1 T_2)$ , respectively. In these expressions,  $d_0$  is the transition dipole matrix element,  $T_2$  is the atomic dephasing time,  $N_T$  is the total density of the dopants,  $\varepsilon_0$  is vacuum permittivity, and  $\hbar$  is Planck's constant divided by  $2\pi$ . From Eq. (9), we can see that the imaginary and the real parts of the susceptibility are related through  $\text{Re}(\chi) = -(\omega - \omega_0)T_2 \text{Im}(\chi)$ . Using this relation and Eq. (9), we can reduce the conditions in Eq. (8) to

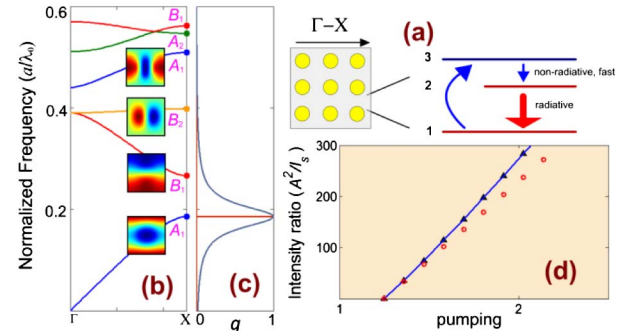


Fig. 1. (a) Schematic of 2D PC and the active dopant. (b) The band structure of  $E$  polarization. The insets show the magnitude of the magnetic field (whose components are in the 2D periodic plane) for the modes at the  $X$  point. The modes at  $X$  are labeled with their symmetry representations. (c) The gain line shape function of  $\text{Er}^{3+}$  (red curve), and for an active medium that has 1000 times larger line width than that of  $\text{Er}^{3+}$  (dark blue). (d) The intensity ratio as a function of pumping for the first Bloch mode (with symmetry representation  $A_1$ ). Blue line: exact self-consistent method [5]; open circles: perturbation theory [6]; triangles: presented method.

$$\omega_m^2/\omega^2 = 1 + (\omega - \omega_0)\langle\gamma\psi^2\rangle T_2. \quad (10)$$

The density of the dopants is in the excited state (i.e., level 2)  $N = N_T(p - 1)/(p + 1)$ . The minimum  $N$  required for gain to offset loss, and hence induce a steady-state lasing, is defined as the threshold dopant density,  $N_{\text{th}}$ . The expression for  $N_{\text{th}}$  can be obtained from the first condition in Eqs. (8) and (9) with  $A = 0$ :

$$N_{\text{th}} = \frac{\langle\gamma\psi^2\rangle}{g_0\langle\eta\psi^2\rangle} [1 + (\omega - \omega_0)^2 T_2^2]. \quad (11)$$

From Eq. (10), we can see that the steady-state mode frequency,  $\omega$ , does not depend on the pumping level, but does depend on the loss, [or equivalently on  $N_{\text{th}}$ , see Eq. (11)]. Since increased pumping will increase the real part of the susceptibility, it is possible that the frequency,  $\omega$ , of the active mode should likewise change with pumping. The real part of the susceptibility depends on the steady-state population inversion density (Eq. (9)). In steady state, for pumping beyond threshold, increasing the pumping value does not change the population inversion density significantly. Instead, energy from the pumping simply deposits more light in the nonlinear Bloch mode (i.e., increase the amplitude  $A$ ). Therefore, in steady state, the population inversion density remains approximately equal to  $N_{\text{th}}$ . Consequently, steady-state frequency,  $\omega$ , remains almost independent of pumping but depends primarily on the loss in the system as seen in Eq. (10). Moreover, when the loss in the system is zero, then  $N_{\text{th}} = 0$  (no change in the susceptibilities), and therefore  $\omega = \omega_m$ . Once  $N_{\text{th}}$  is known, the threshold pumping is then obtained from  $p_{\text{th}} = (N_T + N_{\text{th}})/(N_T - N_{\text{th}})$ . For  $p > p_{\text{th}}$ , the steady-state value of  $A$  is obtained from the nonlinear integral equation:

$$\frac{\langle\gamma\psi^2\rangle(p + 1)}{g_0(p - 1)} = \left\langle \frac{\eta\psi^2}{1 + [(\omega - \omega_0)T_2]^2 + A^2\psi^2(\mathbf{r})/I_s(p + 1)} \right\rangle. \quad (12)$$

Equations 10 through 12 provide excellent approximations for the nonlinear Bloch mode [6,7] frequency and amplitude as well as the threshold pumping for lasing in PCs with three-level active dopants.

We now compare our semi-analytical results with the results of the exact self-consistent method demonstrated in [6]. The active nonlinear structure in [6] consists of a 2D square lattice PC doped with erbium ions ( $\text{Er}^{3+}$ ) [Fig. 1(a)] with only  $E$  polarized (electric field along the axis of rods) light. The 2D PC is made of circular silicon rods (dielectric constant = 12.1 and a radius-to-period ratio of 0.3) in a silicon dioxide matrix (dielectric constant = 2.1). The band structure of the backbone PC along the  $\Gamma$ - $X$  direction is shown in Fig. 1(b).  $\text{Er}^{3+}$  ions with the following parameters:  $g_0 = 5.9 \times 10^{-5}$  at density  $N_T = 1 \times 10^{19} \text{ cm}^{-3}$ , resonance wavelength,  $\lambda_0 = 1.5$  microns, and  $T_2 = 5.6$  ps, are doped in the  $\text{SiO}_2$  matrix region. The loss in the silicon rods (due to out-of-plane scattering and impurity absorption) is parameterized by  $\gamma = 1 \times 10^{-5}$ . For suitable pumping conditions, lasing takes place along

the  $\Gamma$ - $X$  direction at the band edge ( $X$ ). We choose the PC lattice constant,  $a$ , such that the resonance frequency,  $\omega_0 = a/\lambda_0$ , is close (within one full width at half-maximum) to the first band edge at  $X$  with  $\omega_m = 0.1856$ . The gain line shape function (related to  $\text{Im}(\chi)$  for  $A = 0$ ),  $g = 1/\{1 + [(\omega - \omega_0)T_2]^2\}$ , of  $\text{Er}^{3+}$  is plotted in Fig. 1(c).

Before proceeding, we justify the single-mode assumption made earlier. The magnitude of the gain line shape function ( $g$ ) is an indicator of the coupling strength of our dopants to modes of the backbone PC. On the other hand, the coupling between different backbone modes induced by the active medium is strongly dependent on the symmetry of the modes. It was shown previously [6] that Bloch modes with different wave-vectors remain uncoupled provided that the active medium has the same translational symmetry as the backbone. The same is true for the point group symmetries. In Fig. 1(b), the  $X$ -point modes are labeled with their respective symmetry representation [17]. The symmetry representation tells us whether the mode is symmetric or antisymmetric with respect to the symmetry operations of the point group at  $X$ . For example, the modes with  $A_1$  representation are symmetric with respect to all symmetry operations (identity,  $180^\circ$  rotation, mirror operations along horizontal and vertical axes) of the point group  $C_{2v}$  (the symmetry group of  $X$ ). It can be shown that only modes with the same symmetry representation couple to each other [18]. As we can see from Fig. 1(c), the line width of  $\text{Er}^{3+}$  is very narrow, and thus the coupling to all other modes with the same Bloch wave-vector is correspondingly small. Although the second and third bands have finite  $g$  values, these neighboring modes do not have the same symmetry representation as the lowest band edge mode. Consequently, these neighboring modes will not couple to the first band edge mode. Among the first six bands, only the band edge mode of the fourth band has the same symmetry as that of the first band. However, the coupling strength to this band (due to the narrow dopant linewidth) is nearly zero. Therefore, the single-mode assumption is valid for any practical purposes in this example.

The presented transient and steady-state Eqs. (7) and (8) work very well provided that the single-mode assumption is justified. A straightforward multimode generalization is required if (1) the symmetries of the active medium (both translational and point group) are not the same as those of the backbone structure or (2) an inhomogeneous linewidth of active dopants or gain rate is a significant fraction of the spectral separation between modes of the same symmetry.

In Fig. 1(d), we compare the result of exact computation [6] (blue line) to the solutions of Eq. (12) (triangles) for the intensity ratio ( $A^2/I_s$ ). Clearly, there is near perfect agreement between the two methods. Whereas the exact method involves self-consistent diagonalization of a large matrix, Eq. (12) is simply solved using a bisection method. The value of  $p_{\text{th}}$  is also analytically obtained from Eq. (11). This is simpler than the exact method, where  $p_{\text{th}}$  is found by an iterative numerical approach. For comparison, we also plot the result of a multiscale perturbation theory [8] (circles) in Fig. 1(d). Clearly, the perturbation theory is only valid near threshold as expected.

In conclusion, we have demonstrated a simple semi-analytical technique to accurately describe a macroscopic response in active nonlinear optical nanostructures. This simplifies the description of nonlinear Bloch waves and lasing in 2D and 3D PCs to an effective 1D problem for the slowly varying, macroscopic, wave amplitudes. Our method recaptures previous self-consistent iterative solutions [6] of microscopic wave equations in periodic media with frequency-dependent, nonlinear, dielectric functions, exhibiting gain and loss. Our approach provides a vital method in more complex nanostructures, such as electrically pumped 3D metallic, PC, filaments [19] and PC solar cells [20] with electron-hole luminescence (photon-recycling) effects. In both systems, nonlinear Bloch waves and lasing may arise with sufficiently strong pumping, but exact microscopic treatments are prohibitively time-consuming.

This work was supported by the United States Department of Energy under contract DE-FG02-10ER46754, the Agency for Science, Technology and Research (A-STAR) of Singapore, and the Natural Sciences and Engineering Council of Canada.

#### References and Note

1. B. Ellis, M. A. Mayer, G. Shambat, T. Sarmiento, J. Harris, E. E. Haller, and J. Vučković, *Nat. Photonics* **5**, 297 (2011).
2. S. Strauf, K. Hennessy, M. T. Rakher, Y.-S. Choi, A. Badolato, L. C. Andreani, E. L. Hu, P. M. Petroff, and D. Bouwmeester, *Phys. Rev. Lett.* **96**, 127404 (2006).
3. P. Bermel, E. Lidorikis, Y. Fink, and J. D. Joannopoulos, *Phys. Rev. B* **73**, 165125 (2006).
4. S. L. Chua, Y. Chong, A. D. Stone, M. Soljacic, and J. B. Abad, *Opt. Express* **19**, 1539 (2011).
5. H. Takeda and S. John, *Phys. Rev. A* **83**, 053811 (2011).
6. A. Kaso and S. John, *Phys. Rev. E* **74**, 046611 (2006).
7. A. Kaso and S. John, *Phys. Rev. A* **76**, 053838 (2007).
8. L. Florescu, K. Busch, and S. John, *J. Opt. Soc. Am. B* **19**, 2215 (2002).
9. R. W. Boyd, *Nonlinear Optics*, 3rd ed. (Academic, 2008), Chap. 3.
10. M. Sargent III, M. O. Scully, and W. E. Lamb, *Laser Physics* (Addison-Wesley, Reading, Mass, 1977), Chap. 8.
11. A. E. Siegman, *Lasers* (University Science Books, 1986), Chap. 24, Sect. 4.
12. In the semiclassical laser theory  $\partial A/\partial t$  and the loss ( $\sigma$ ) are both assumed one order smaller than  $\omega A$  and are referred to as first-order terms (Refs. [10,11]). Their product,  $A/\partial t$ , is a second-order term that can be neglected. A more systematic ordering and elimination of second-order terms can be accomplished by a multiscale expansion method as discussed in [8].
13. C. M. de Sterke and J. E. Sipe, *Phys. Rev. A* **38**, 5149 (1988).
14. C. M. Bowden and G. P. Agrawal, *Opt. Commun.* **100**, 147 (1993).
15. Y. C. Lan, *Appl. Phys. Lett.* **88**, 071109 (2006).
16. P. W. Milonni and J. H. Eberly, *Laser Physics*, 2nd ed. (Wiley, 2010).
17. K. Sakoda, *Phys. Rev. B* **52**, 7982 (1995).
18. J. F. Cornwell, *Group Theory in Physics* (Academic, 1997).
19. S. John and R. Wang, *Phys. Rev. A* **78**, 043809 (2008).
20. S. Eyderman, S. John, and A. Deinega, *J. Appl. Phys.* **113**, 154315 (2013).